Structural basis for glutathione-mediated activation of the virulence regulatory protein PrfA in *Listeria*

Michael Hall[a,b], Christin Grundström[a,b], Afshan Begum[a,b], Mikael J. Lindberg[a,b], Uwe H. Sauer[a,b], Fredrik Almqvist[a,b], Jörgen Johansson[b,c,d], and A. Elisabeth Sauer-Eriksson[a,b,1]

[a]Department of Chemistry, Umeå University, 901 87 Umeå, Sweden; [b]Umeå Centre for Microbial Research, Umeå University, 901 87 Umeå, Sweden; [c]Department of Molecular Biology, Umeå University, 901 87 Umeå, Sweden; and [d]Molecular Infection Medicine Sweden, Umeå University, 901 87 Umeå, Sweden

Edited by Pascale Cossart, Institut Pasteur, Paris, France, and approved November 17, 2016 (received for review August 22, 2016)

Infection by the human bacterial pathogen *Listeria monocytogenes* is mainly controlled by the positive regulatory factor A (PrfA), a member of the Crp/Fnr family of transcriptional activators. Published data suggest that PrfA requires the binding of a cofactor for full activity, and it was recently proposed that glutathione (GSH) could fulfill this function. Here we report the crystal structures of PrfA in complex with GSH and in complex with GSH and its cognate DNA, the *hly* operator PrfA box motif. These structures reveal the structural basis for a GSH-mediated allosteric mode of activation of PrfA in the cytosol of the host cell. The crystal structure of $PrfA_{WT}$ in complex only with DNA confirms that $PrfA_{WT}$ can adopt a DNA binding-compatible structure without binding the GSH activator molecule. By binding to PrfA in the cytosol of the host cell, GSH induces the correct fold of the HTH motifs, thus priming the PrfA protein for DNA interaction.

PrfA | glutathione | activation | *Listeria* | virulence

The Gram-positive bacterium *Listeria monocytogenes* is a saprophyte and a pathogen responsible for the severe disease listeriosis in humans on ingestion (1, 2). Its ability to grow at low temperatures and in high-salt and low-oxygen conditions makes *L. monocytogenes* one of the most problematic foodborne pathogens. Pregnant women, immunocompromised persons, and other at-risk individuals are more vulnerable to invasive listeriosis, and the high mortality rates in these subpopulations (~20–40%) demonstrate the clinical difficulty in dealing with these infections (1, 3–6).

The expression of key virulence factors necessary for infection by the human bacterial intracellular pathogen *L. monocytogenes* is controlled by the transcriptional activator PrfA, a member of the Crp/Fnr family (7–10). The list of identified Crp/Fnr family regulators is growing with the increasing number of whole bacterial genome sequences (11); however, for many of them, the functions are not well defined. Whereas most Crp family members require a small-molecule cofactor for DNA binding, PrfA is capable of binding to its consensus DNA sequence with low affinity even in the absence of a cofactor (12). Nonetheless, the activity of PrfA is known to increase in the intracellular environment, which suggests that its activation is regulated by a host-derived or host-regulated cofactor (2, 13). An allosteric mode of PrfA activation is further supported by crystal structures in which the constitutively active PrfA mutant $PrfA_{G145S}$ positions the winged helix-turn-helix (HTH) motif in an ordered and exposed "active" conformation, in contrast to $PrfA_{WT}$, where the HTH motif remains partially disordered (12, 14).

It was recently suggested that reduced glutathione (GSH) can function as a cofactor for PrfA, thereby increasing the activity of PrfA at target genes (15, 16). Based on a genetic selection approach, *gshF* in *L. monocytogenes*, encoding a glutathione synthase, was shown to be essential for PrfA activity (15). Further work showed that reduced glutathione (GSH) could function as cofactor for PrfA, increasing the activity of PrfA at target genes (15, 16). To elucidate the structural basis for allosteric activation by GSH, we determined the crystal structures of GSH bound to $PrfA_{WT}$ and of $PrfA_{WT}$ in complex with GSH as well as its operator DNA. The structures clearly show how GSH bound at the PrfA tunnel site stabilizes the HTH fold, thus increasing the ratio of active DNA-binding PrfA proteins over the inactive ones.

Results and Discussion

Binding of Glutathione to PrfA Induces Formation of the HTH Motif. Structurally, each monomer of PrfA comprises an N-terminal eight-stranded β-barrel domain connected by an α-helix linker to a C-terminal α/β domain (12, 14). The C-terminal region contains the HTH motif responsible for binding to target DNA operators with the 14-bp palindromic "PrfA box" consensus sequence (TTAACANNTGTTAA) (12, 14). The asymmetric unit of the $PrfA_{WT}$-GSH complex crystals contains four biological dimers: monomers A–H. Difference Fourier and anomalous electron density maps confirmed the binding of GSH to $PrfA_{WT}$ in all monomers (Fig. 1 *A–D* and Table 1). The electron density for the entire GSH molecule is unambiguous in monomers A–D. In monomers E–H, however, the glutamate and glycine groups of GSH are less well defined, with structural consequences that we discuss below.

In all monomers, GSH binds at an intraprotein tunnel site, located between the N- and C-terminal domains of the monomer (Fig. 1 *B* and *C*). This region was recently identified by us as a binding site for a PrfA inhibitor based on ring-fused 2-pyridones (17), and also has been identified as a putative cofactor binding site (2, 12). In monomers A–D, GSH binds as an additional β-strand to the protein by making five main-chain contacts to β5 and the turn connecting to β6 (residues Tyr62–Ala66) (Fig. 1 *C* and *E* and Fig. S1). The thiol group of GSH is buried in a hydrophobic pocket formed by the side chains of Tyr126 (positioned on αC), Tyr63(β5), Phe67(β5), and Trp224(αH). The deep end of the pocket is formed by Gln61(β5) and Gln123(αC) connected by hydrogen bonds. The carboxyl group of the GSH glutamate forms an electrostatic interaction with

Significance

Infection by the human bacterial pathogen *Listeria monocytogenes* is controlled mainly by the transcriptional activator PrfA, a member of the Crp/Fnr family. Here we report the crystal structures of PrfA in complex with glutathione (GSH) and in complex with GSH and its cognate DNA, the *hly* operator PrfA box motif. The structures provide detailed information and insight into how GSH interacts with PrfA and thus induces the correct fold of the HTH motif promoting PrfA DNA binding.

Author contributions: M.H. and A.E.S.-E. designed research; M.H., C.G., A.B., M.J.L., U.H.S., and A.E.S.-E. performed research; M.H. and A.E.S.-E. analyzed data; and M.H., U.H.S., F.A., J.J., and A.E.S.-E. wrote the paper.

The authors declare no conflict of interest.

This article is a PNAS Direct Submission.

Freely available online through the PNAS open access option.

Data deposition: The atomic coordinates and structure factors have been deposited in the Protein Data Bank, www.pdb.org (PDB ID codes 5LRR for PrfAWT-GSH, 5LRS for PrfAWT-GSH-DNA, 5LEJ for PrfAWT-DNA, and 5LEK for PrfAG145S-DNA).

[1]To whom correspondence should be addressed. Email: elisabeth.sauer-eriksson@umu.se.

This article contains supporting information online at www.pnas.org/lookup/suppl/doi:10.1073/pnas.1614028114/-/DCSupplemental.

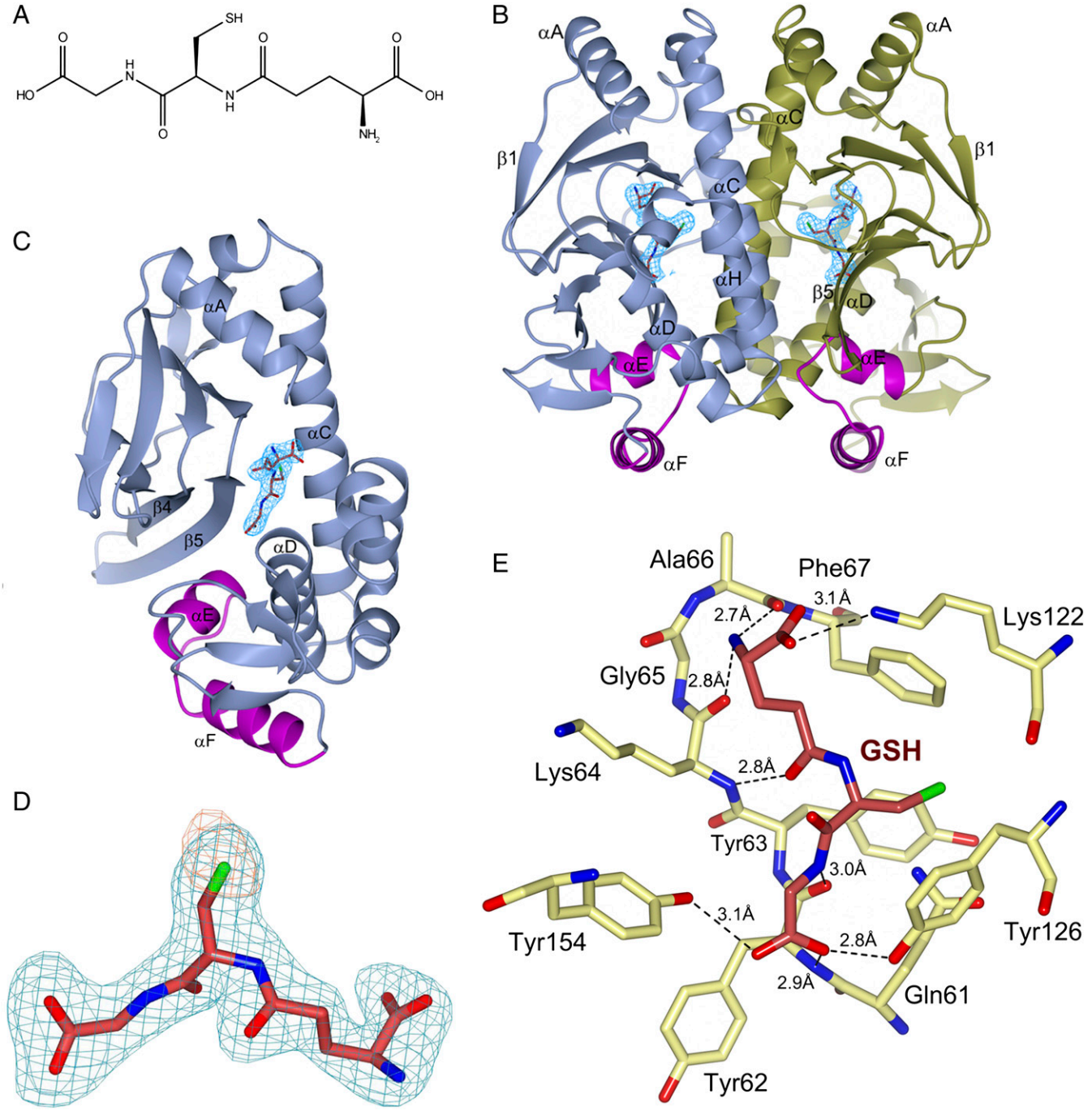

Fig. 1. Structure of $PrfA_{WT}$ in complex with GSH. (*A*) Chemical structure of GSH. (*B*) Ribbon representation of the $PrfA_{WT}$ homodimer showing the binding sites of GSH at the tunnel site of each monomer. The monomers A and B are colored in blue and gold, respectively. The HTH motif is highlighted in magenta, and GSH is shown as sticks with carbon atoms colored crimson. The difference (2|Fo|-|Fc|) electron density map calculated from the refined PrfA-GSH complex and contoured at the RMSD value of the map is shown in blue covering GSH only. (*C*) Alternative orientation of *B* showing monomer A only. (*D*) Representative electron density covering the refined model of GSH in monomer A. An unbiased difference (|Fo|-|Fc|) electron density map contoured at three times the RMS value of the map is shown in blue. To reduce model bias, the GSH molecule was excluded from the coordinate file that was subjected to refinement before calculation of the electron density map. The anomalous log-likelihood-gradient (LLG) map, in orange, shows the position of the sulfur atom of GSH. (*E*) Key local structural features and amino acids forming direct hydrogen bonds (dashed lines) to GSH in monomer A. Gln123 and Trp224 are not shown for clarity. Additional structural features in the vicinity of the GSH-binding site are shown in Fig. S1.

Lys122(αC) and is positioned ~4 Å from the SH group of Cys229(αH). The backbone nitrogen atom of Lys64(β5) hydrogen bonds to GSH; however, its side chain does not contact the cofactor, but rather makes a hydrogen bond to the main-chain carbonyl oxygen of Val153(αD). Both Lys122 and Lys64 are known to affect the activation of PrfA (18), in agreement with their observed binding pattern.

At the glycine end of GSH, the carboxyl group of glycine is positioned in the vicinity of the HTH motif, forming hydrogen bonds to the hydroxyl groups of Tyr126(αC) and Tyr154(αD)

Table 1. Data collection and refinement statistics

Data	$PrfA_{WT}$-GSH	$PrfA_{WT}$-GSH-DNA	$PrfA_{WT}$-DNA	$PrfA_{G145S}$-DNA
Data collection				
Space group	$P2_12_12$	$P4_32_12$	$P4_32_12$	$P4_32_12$
Cell dimensions				
a, *b*, *c*, Å	116.3, 184.3, 100.5	78.9, 78.9, 265.2	79.1, 79.1, 265.8	79.1, 79.1, 266.0
α, β, γ,°	90, 90, 90	90, 90, 90	90, 90, 90	90, 90, 90
Resolution, Å	48.5–2.17 (2.25–2.17)	58.9–2.90 (3.08–2.90)	47.3–2.70 (2.83–2.70)	47.3–2.80 (2.95–2.80)
R_{merge}	0.123 (1.840)	0.176 (1.218)	0.089 (1.184)	0.091 (1.281)
$I/\sigma I$	13.2 (1.5)	16.0 (3.1)	16.8 (1.9)	14.0 (1.7)
Completeness, %	99.6 (96.7)	99.5 (99.8)	99.8 (99.4)	99.4 (99.2)
Redundancy	13.4 (13.1)	25.6 (26.2)	8.6 (8.6)	7.0 (6.9)
Refinement				
No. of reflections	113,941 (11,013)	19,373 (1,898)	24,171 (2,338)	21,615 (2,099)
R_{work}	0.208 (0.310)	0.249 (0.350)	0.230 (0.323)	0.231 (0.378)
R_{free}	0.240 (0.351)	0.281 (0.366)	0.266 (0.436)	0.267 (0.435)
No. of atoms				
Protein	15,277	3,840	3,848	3,844
DNA	–	1,224	1,224	1,224
GSH/Na^+/PI	160/5/15	40/0/0	0/0/0	0/0/0
Water	504	15	7	3
B-factors, $Å^2$				
Protein	57.6	72.6	65.8	81.8
DNA	–	73.7	70.7	93.6
GSH/Na^+/PI	59.5/44.3/89.4	50.9/–/–	–/–/–	–/–/–
Water	50.1	40.7	39.1	46.0
RMSD				
Bond lengths, Å	0.003	0.003	0.003	0.004
Bond angles,°	0.48	0.56	0.51	0.76

For each structure, diffraction data were collected on a single crystal. Values in parentheses are for the highest-resolution shell. Resolution limits were determined by applying a cutoff based on the mean intensity correlation coefficient of half-datasets, $CC_{1/2}$. PI, hydrogen phosphate ion.

and water-mediated hydrogen bonds to the Oγ atom of Ser177 in the HTH motif (Fig. S1). Previous studies have implicated Tyr154 in the activation of PrfA, where a Tyr154-to-Cys substitution, like $PrfA_{WT}$, promotes a modest increase in extracellular PrfA-dependent gene expression. However, in contrast to $PrfA_{WT}$, the Y154C mutation inhibits host cytosol-mediated induction of virulence genes (19). Furthermore, the backbone torsion angles of the GSH tripeptide are in an extended β-strand conformation, allowing it to make five main-chain contacts with strands β5 and the turn connecting to β6 (Fig. 1*E*). Combined, these interactions lead to the collapse of the tunnel, which is needed for the formation of the activated structure of PrfA (Fig. 2) (12).

Interestingly, in two of the four dimers within the asymmetric unit of the $PrfA_{WT}$-GSH crystal structure (i.e., dimers EF and GH), the GSH molecules are bound via their thiol groups in the hydrophobic pocket with weak electron density covering the glutamate and glycine parts of the molecules, which suggests flexibility of the ligands. Consequently, their HTH motifs are only partially folded, and for monomers F and H, the HTH loop is as flexible as in the $PrfA_{WT}$ apo structure [Protein Data Bank (PDB)

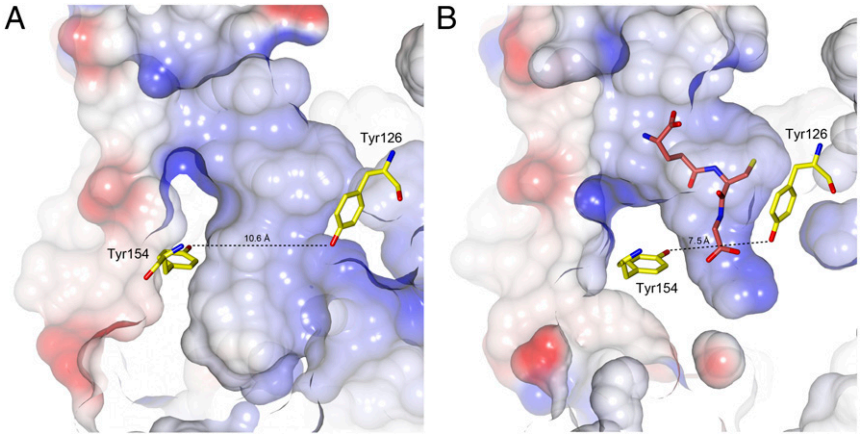

Fig. 2. Shape of the tunnel site in $PrfA_{WT}$ (PDB ID code 2BEO) (*A*) and $PrfA_{WT}$ with bound GSH (*B*). The cofactor and protein atoms are color-coded as in Fig. 1*E*. The figure highlights the effects of the major conformational changes that occur at the tunnel site following binding of GSH. The conformational changes diminish the size of the tunnel, particularly at the glycine end of the ligand, leading to stable formation of the HTH motif (not shown).

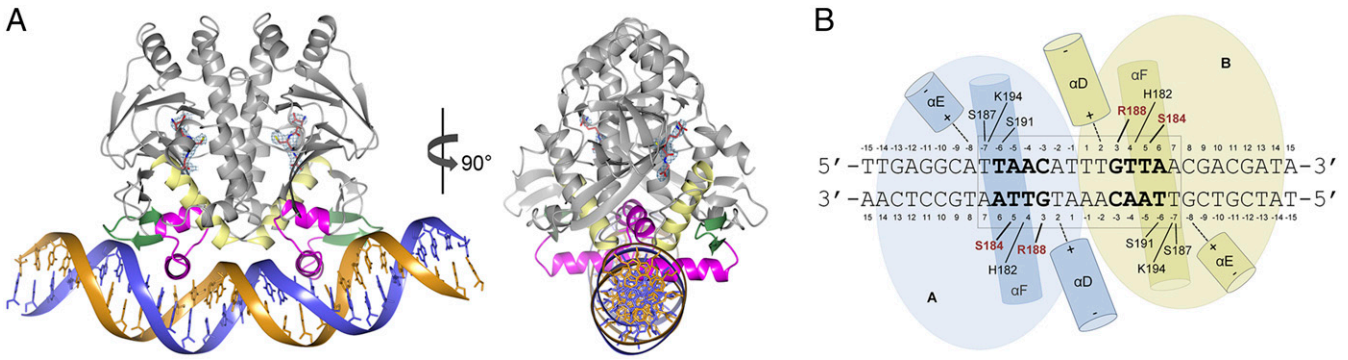

Fig. 3. Structure of the $PrfA_{WT}$-GSH-DNA complex. (*A*) Ribbon representation of the DNA-bound homodimer showing the binding sites of GSH at the tunnel site of each monomer. The monomers A and B are colored in gray, the HTH motif is in magenta, αD is in yellow, and the winged β-hairpin is in green. GSH is shown as sticks with the carbon atoms in crimson. The electron density covering the GSH molecules is calculated as in Fig. 1*B*. The 30-bp palindromic operator is shown in dark blue and orange. (*B*) Schematic drawing of the $PrfA_{WT}$-DNA interactions. The two residues that make base-specific contacts are highlighted in red. Other contacts are nonspecific interactions between protein side chains and the DNA phosphate backbone.

ID code 2BEO] (12). This shows that simply binding of GSH in the tunnel is not sufficient for activation—all three residues in GSH must be properly oriented to induce the active conformation of the HTH motif. Furthermore, to stabilize both HTH motifs in the active conformation within the $PrfA_{WT}$ dimer, two GSH molecules must bind correctly, one for each monomer.

Glutathione-Activated PrfA Is Primed for DNA Binding. Superimposition of the 237 alpha-carbon atoms of the $PrfA_{WT}$-GSH complex onto the $PrfA_{WT}$ and the constitutively active PrfA mutant $PrfA_{G145S}$ structures results in RMSD values of 1.47 Å and 0.52 Å, respectively. The latter value shows that binding of GSH transformed $PrfA_{WT}$ into a structure very similar to the constitutively active mutant structure, primed for DNA binding. To confirm this observation, we determined the crystal structure of $PrfA_{WT}$ in complex with GSH and a 30-bp fragment corresponding to the PrfA box region of the *hly* operator (Fig. 3*A*, Table 1, and Fig. S2). Superimposition of the $PrfA_{WT}$-GSH and $PrfA_{WT}$-GSH-DNA complexes showed that no additional changes to the $PrfA_{WT}$-GSH structure occur when bound to DNA (RMSD of monomer A, 0.52 Å, and of monomer B, 0.41 Å, superimposing 234 Cα atoms; RMSD of dimers AB, 0.54 Å, superimposing 468 Cα atoms). This implies that the $PrfA_{WT}$-GSH structure is primed for DNA binding via direct docking to the operator DNA with only minimal conformational changes to the protein. However, on binding to activated $PrfA_{WT}$, DNA bends by ∼30°.

DNA bending can play a role in transcription activation, and the bent DNA structure observed here is in agreement with the three previously determined structures of complexes between Crp/Fnr family members and DNA: Crp from *Escherichia coli* (PDB ID code 1CGP) (20), CprK from *Desulfitobacterium* spp. (PDB ID code 3E6C) (21), and $FixK_2$ from *Bradyrhizobium japonicum* (PDB ID code 4I2O) (22). In these three cases, the DNA molecules are bent at 90°, 90°, and 55°, respectively (Fig. S3). It is possible that $PrfA_{WT}$ needs an additional cofactor to accomplish further bending of DNA for full transcriptional activation. As predicted, DNA binding is mediated via the preformed HTH motif that was previously identified in the $PrfA_{G145S}$ mutant structure (12) and now has been found in the activated $PrfA_{WT}$-GSH structure as well. Residues that constitute the HTH motif include PrfA, αE (H_1), Met171-Gly179; turn, Ile180-His182; and the recognition helix αF (H_2), Ser183-Lys197. PrfA makes both base-specific hydrogen bonds and nonspecific hydrogen bonds or charge–charge contacts with DNA.

The helices αD and αE are positioned perpendicular to the axis of the DNA helix and make electrostatic interactions through their N-cap amino groups to the phosphate backbone of T+2 and A-8, respectively. Perpendicular to these two helices lies the recognition helix αF in the major groove of the operator DNA (Fig. 3*B*). Two base-specific interactions are formed between Ser184 and Arg188 and the bases of T+5 and G+3, respectively (Fig. 4). Additional nonspecific charge–charge or hydrogen bonds between protein side chains and phosphate backbone groups include His182 to T+4, Ser187 to T-7, and Lys194 to T-7. Contacts between the winged β-hairpin (β-strands 13 and 14), composing residues Ile199–Gln209, are not clearly defined; however, there is evidence of a water-mediated contact between the side chain of Tyr-201 and the phosphate group of A-8.

Structural Mechanism of GSH-Mediated PrfA Activation. The molecular basis for PrfA activation can be readily explained by the GSH-induced conformational changes (Fig. 5 *A* and *B*). The binding affinity of GSH to PrfA is ∼4 mM, a relatively low value for an activator molecule (15); however, both prokaryotes and eukaryotes maintain estimated intracellular concentrations of 0.1–10 mM glutathione (23–25), demonstrating that the measured binding affinity is within a biologically relevant range (15). The genetic selection method used to identify GSH as a cofactor suggests that GSH comes mainly from the bacteria (15). By binding to PrfA in the cytosol of the host cell, GSH induces the correct fold of the HTH motifs, thus increasing the ratio of DNA binding-enabled PrfA proteins over the inactive ones (Fig. 5*C*). The bending of DNA in the $PrfA_{WT}$-GSH-DNA structure of ∼30° is less pronounced

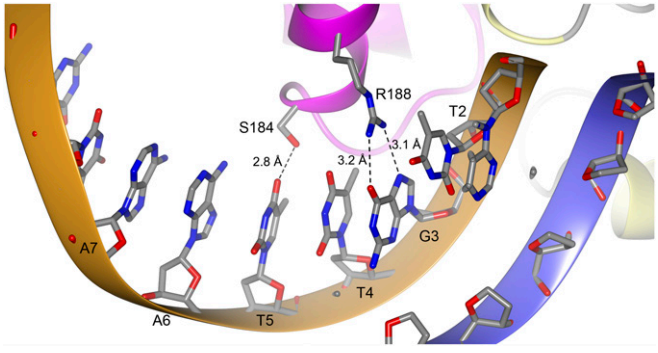

Fig. 4. Close-up view of base-specific contacts. The side chains of Ser184 and Arg188 from monomer A form hydrogen bonds to T+5 and G+3, respectively. The hydrogen bonds are indicated by dashed lines. The same hydrogen bonds are present in monomer B. For clarity, only bases from one strand of DNA are shown.

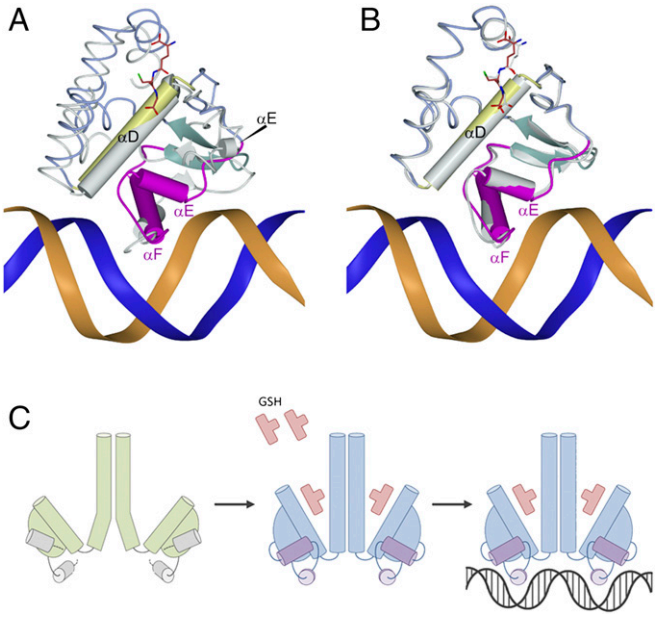

Fig. 5. Allosteric GSH binding primes PrfA for DNA binding. (*A* and *B*) Superimposition of the $PrfA_{WT}$-GSH-DNA with $PrfA_{WT}$ (PDB ID code 2BEO) (*A*) and the $PrfA_{WT}$-GSH complex (*B*). $PrfA_{WT}$-GSH-DNA is color coded as in Fig. 2*A*. The other structures are shown in gray. Superimposition is based on C-terminal residues only (amino acids Y126-N237). (*C*) A molecular model for GSH-mediated activation of PrfA based on the structures of GSH bound to *L. monocytogeneses* $PrfA_{WT}$, with and without operator DNA. Allosteric binding of GSH to the tunnel site of $PrfA_{WT}$ changes the conformation of residues at the DNA-binding C-terminal domain and leads to formation of the HTH motifs, thereby locking the PrfA dimer in the active conformation that readily docks into its operator DNA.

than that in other DNA-bound Crp/Fnr family members of known structure. It is possible that another factor or regulatory protein is required for full DNA bending and activation.

Because $PrfA_{WT}$ is known to interact with DNA even in the absence of an activator, we determined the crystal structures of the $PrfA_{WT}$-DNA and the $PrfA_{G145S}$-DNA complexes in the absence of GSH (Table 1). Both structures are almost identical to the $PrfA_{WT}$-GSH-DNA complex structure. Superimposition of the Cα backbone of the $PrfA_{WT}$-GSH-DNA model with the Cα backbones of $PrfA_{WT}$-DNA and $PrfA_{G145S}$-DNA resulted in low RMSD values of 0.35 Å and 0.25Å, respectively. The $PrfA_{WT}$-DNA structure confirms that $PrfA_{WT}$ can adopt a DNA binding-compatible structure without binding the GSH activator molecule.

Other Crp/Fnr family members, such as Crp in *E. coli*, use cAMP for activation (26). In *E. coli*, cAMPs bind at the N-terminal domain of both Crp monomers, where the antiparallel β-roll structure composes part of the cAMP binding site (27). Whereas the cAMP binding site is topologically conserved within the N-terminal domain of PrfA, the residues involved in cAMP binding are not (12). The crystal structure of the $PrfA_{WT}$-GSH complex shows that GSH does not bind at the conserved Crp-cAMP binding site (Fig. 6). The key amino acids for GSH binding are not conserved among the Crp/Fnr family members. Furthermore, binding of activator molecules in the tunnel has not been observed among homologous proteins. This observation supports previous notions that despite the significant structural similarity between its members, a distinct allosteric mechanism is the key strategy for this protein family to control a wide range of biological processes (20–22).

Materials and Methods

Expression, Purification, and Crystallization. Using 5′ NcoI and 3′ Acc651 restriction sites, the PrfA gene was cloned into a modified pET24d plasmid containing an upstream, in frame coding region for a 6-His tag and a Tobacco etch virus (TEV) protease cleavage site (17). The construct encodes the full-length $PrfA_{WT}$ protein (M1-N237) and results in the addition of two nonnative N-terminal residues (GA) on TEV cleavage. Creation of the $PrfA_{G145S}$ construct was performed with the QuikChange Site-Directed Mutagenesis Kit (Agilent), using the plasmid described above as a template. The protein was overexpressed in *E. coli* BL21 (DE3) plysS (Novagen) cells. Cultures were grown at 310 K in LB medium supplemented with 50 μg mL^{-1} kanamycin and 34 μg mL^{-1} chloramphenicol to an OD_{600} of 0.6, at which point protein expression was induced by the addition of isopropyl β-D-1-thiogalactopyranoside to a final concentration of 0.4 mM, and continued growth overnight at 293 K. Cells were harvested by centrifugation and lysed by sonication on ice. Purification of $PrfA_{WT}$ for crystallization in the absence of DNA was performed as described previously (17), but with the addition of a final size-exclusion chromatography step performed in a HiLoad Superdex 75 16/60 column (GE Healthcare) equilibrated with 20 mM sodium phosphate pH 6.5, and 200 mM NaCl.

$PrfA_{WT}$ and $PrfA_{G145S}$ proteins used for crystallization in complex with DNA were purified on a 5-mL HisTrap HP nickel-affinity column in lysis buffer containing 20 mM Tris·HCl pH 8.0, 20 mM imidazole, and 500 mM NaCl. Samples bound to the column were washed with 10 column volumes of lysis buffer and then eluted with a linear gradient of 20–500 mM imidazole. The polyhistidine tag was removed by overnight cleavage with TEV protease. Cleaved target proteins were separated from 6-His–tagged TEV protease, 6-His–tagged fragments, and uncleaved target proteins by nickel-affinity chromatography as described above. The final step in $PrfA_{WT}$ and $PrfA_{G145S}$ purification was done by size-exclusion chromatography using a HiLoad Superdex 200 16/60 column (GE Healthcare) equilibrated with 20 mM Tris·HCl pH 8.0 and 150 mM NaCl. The purity of the proteins as assessed by SDS/PAGE was >95%.

Each protein was concentrated using an Amicon Ultra centrifugal filter device (Millipore) before being flash- cooled in liquid N_2 and stored at −80 °C. Two complementary 30-bp DNA oligonucleotides, representing the *hly* PrfA box motif, were purchased from Eurofins Genomics (5′-TTGAGGCATTAACATTTGT-TAACGACGATA-3′, reverse complement: 5′-TATCGTCGTTAACAAATGTTAATG-CCTCAA-3′) and annealed by slow cooling from 95 °C to room temperature over 3 h in 10 mM Tris·HCl pH 8.0, 50 mM NaCl, and 1 mM EDTA to form a blunt-ended DNA duplex. $PrfA_{WT}$ in complex with GSH was crystallized by the hanging-drop vapor-diffusion method in VDX plates (Hampton Research) at 291 K. Before the crystallization setup, GSH and DTT were added to the protein solution to a final concentration of 5 mM and 1 mM, respectively. Droplets of 4 μL of protein solution at 3 mg mL^{-1} were mixed with 2 μL of reservoir solution consisting of 22% PEG 4000 and 100 mM sodium citrate pH 5.5. Crystals used for data collection were obtained after 48 h.

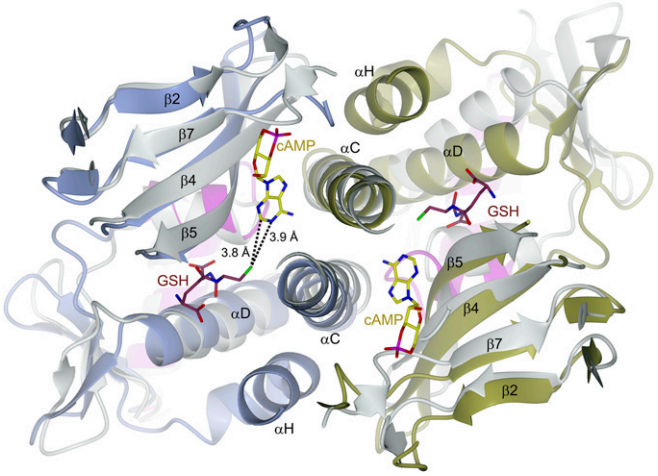

Fig. 6. Superposition of the $PrfA_{WT}$-GSH (monomers A and B shown in blue and gold, respectively) and the Crp-cAMP complexes (gray; PDB ID code 1G6N) based on monomer A (194 aligned Cα atoms with an RMS distance of 1.9 Å). The closest distances between GSH and cAMP in the superimposed monomers are indicated.

Before vitrification, crystals were equilibrated for 24 h in a solution containing 30% PEG 4000, 100 mM sodium citrate pH 5.5, and 50 mM GSH. For crystallization of $PrfA_{WT}$-DNA and $PrfA_{G145S}$-DNA complexes, protein and duplex DNA were incubated together at a ratio of 1:1.3 (PrfA dimer:hly DNA) at a final concentration of 50 μM and 70 μM, respectively, in 20 mM Tris·HCl pH 8.0, 150 mM NaCl, and 1 mM DTT for 60 min at room temperature, before being used for the crystal setups. Crystals were obtained after 24 h by mixing 4 μL of protein-DNA solution with 2 μL of reservoir solution consisting of 8% PEG 8000, 100 mM sodium acetate pH 4.6, 100 mM magnesium acetate, and 20% glycerol. Crystals of $PrfA_{WT}$-DNA and $PrfA_{G145S}$-DNA were cryoprotected in reservoir solution containing 30% glycerol. Crystals of $PrfA_{WT}$-DNA in complex with GSH were obtained by soaking $PrfA_{WT}$-DNA crystals in reservoir solution containing 30% glycerol and 100 mM GSH for 24 h.

Data Collection and Refinement. Diffraction data at 100 K were collected at the BESSY ($PrfA_{G145S}$-DNA, BL14.1; $\lambda = 0.9184$ Å) and the ESRF ($PrfA_{WT}$-GSH and $PrfA_{WT}$-GSH-DNA, ID29; $\lambda = 1.0725$ Å, and $PrfA_{WT}$-DNA, ID23-2; $\lambda = 0.8729$ Å). Diffraction images were processed with XDS (28) and scaled and merged using AIMLESS from the CCP4 software suite (29). All structures were determined by molecular replacement with the PHASER program from the PHENIX program suite (30) using the *$PrfA_{G145S}$* structure (PDB ID code 2BGC) (12) as the search model. The atomic models were built manually built using Coot (31) and refined with PHENIX Refine (30). Each chain of the palindromic DNA is numbered from −15 to +15. Initial crystals of the $PrfA_{WT}$-GSH complex could be obtained only at low concentrations (i.e., 5 mM GSH); however, the structure could be only partly determined owing to the low occupancy of the GSH (K_d ∼4 mM) (15). Soaking the initial $PrfA_{WT}$-GSH complex crystals in high concentrations of GSH (50–100 mM) improved crystal quality and fully occupied GSH-binding sites could be identified in the electron density. It is worth noting that a large part of the C-terminal DNA-binding region, including the flexible parts of the HTH motif, is not involved in crystal packing contacts; thus, crystal packing interactions do not prevent GSH from binding or prevent HTH from correctly folding in the crystal. Data collection and refinement statistics are shown in Table 1. Ramachandran outliers are <0.2% for all structures. Figures were prepared with CCP4mg (32).

Data Availability. The atomic coordinates and structure factors have been deposited with the Protein Data Bank (33) (PDB ID codes 5LRR for $PrfA_{WT}$-GSH, 5LRS for $PrfA_{WT}$-GSH-DNA, 5LEJ for $PrfA_{WT}$-DNA, and 5LEK for $PrfA_{G145S}$-DNA).

ACKNOWLEDGMENTS. We thank Drs. C. O. Byrne and Tobias Hainzl for valuable comments. We also thank the staff of the Protein Expertise Platform at Umeå University for cloning services and the beamline staff at the European Synchrotron Radiation Facility (ESRF) and Berlin Electron Storage Ring Society for Synchrotron Radiation (BESSY) for support and access to beamlines ID23-2 and ID29 at ESRF and BL14.1 at BESSY. This work was supported by the K.A. Wallenberg Foundation and the Swedish Research Council.

1. Vázquez-Boland JA, et al. (2001) *Listeria* pathogenesis and molecular virulence determinants. *Clin Microbiol Rev* 14(3):584–640.
2. Freitag NE, Port GC, Miner MD (2009) *Listeria monocytogenes*—from saprophyte to intracellular pathogen. *Nat Rev Microbiol* 7(9):623–628.
3. Hamon M, Bierne H, Cossart P (2006) *Listeria monocytogenes*: A multifaceted model. *Nat Rev Microbiol* 4(6):423–434.
4. Drevets DA, Bronze MS (2008) *Listeria monocytogenes*: Epidemiology, human disease, and mechanisms of brain invasion. *FEMS Immunol Med Microbiol* 53(2):151–165.
5. Jackson KA, Iwamoto M, Swerdlow D (2010) Pregnancy-associated listeriosis. *Epidemiol Infect* 138(10):1503–1509.
6. Kourtis AP, Read JS, Jamieson DJ (2014) Pregnancy and infection. *N Engl J Med* 371(11):1077.
7. Chakraborty T, et al. (1992) Coordinate regulation of virulence genes in *Listeria monocytogenes* requires the product of the prfA gene. *J Bacteriol* 174(2):568–574.
8. Kazmierczak MJ, Wiedmann M, Boor KJ (2006) Contributions of *Listeria monocytogenes* sigmaB and PrfA to expression of virulence and stress response genes during extra- and intracellular growth. *Microbiology* 152(Pt 6):1827–1838.
9. Toledo-Arana A, et al. (2009) The *Listeria* transcriptional landscape from saprophytism to virulence. *Nature* 459(7249):950–956.
10. Cossart P, Lebreton A (2014) A trip in the "New Microbiology" with the bacterial pathogen *Listeria monocytogenes*. *FEBS Lett* 588(15):2437–2445.
11. Matsui M, Tomita M, Kanai A (2013) Comprehensive computational analysis of bacterial CRP/FNR superfamily and its target motifs reveals stepwise evolution of transcriptional networks. *Genome Biol Evol* 5(2):267–282.
12. Eiting M, Hagelüken G, Schubert WD, Heinz DW (2005) The mutation G145S in PrfA, a key virulence regulator of *Listeria monocytogenes*, increases DNA-binding affinity by stabilizing the HTH motif. *Mol Microbiol* 56(2):433–446.
13. de las Heras A, Cain RJ, Bielecka MK, Vázquez-Boland JA (2011) Regulation of *Listeria* virulence: PrfA master and commander. *Curr Opin Microbiol* 14(2):118–127.
14. Vega Y, et al. (2004) New *Listeria monocytogenes* prfA* mutants, transcriptional properties of PrfA* proteins, and structure-function of the virulence regulator PrfA. *Mol Microbiol* 52(6):1553–1565.
15. Reniere ML, et al. (2015) Glutathione activates virulence gene expression of an intracellular pathogen. *Nature* 517(7533):170–173.
16. Reniere ML, Whiteley AT, Portnoy DA (2016) An in vivo selection identifies *Listeria monocytogenes* genes required to sense the intracellular environment and activate virulence factor expression. *PLoS Pathog* 12(7):e1005741.
17. Good JA, et al. (2016) Attenuating *Listeria monocytogenes* virulence by targeting the regulatory protein PrfA. *Cell Chem Biol* 23(3):404–414.
18. Xayarath B, Volz KW, Smart JI, Freitag NE (2011) Probing the role of protein surface charge in the activation of PrfA, the central regulator of *Listeria monocytogenes* pathogenesis. *PLoS One* 6(8):e23502.
19. Miner MD, Port GC, Bouwer HG, Chang JC, Freitag NE (2008) A novel prfA mutation that promotes *Listeria monocytogenes* cytosol entry but reduces bacterial spread and cytotoxicity. *Microb Pathog* 45(4):273–281.
20. Schultz SC, Shields GC, Steitz TA (1991) Crystal structure of a CAP-DNA complex: The DNA is bent by 90 degrees. *Science* 253(5023):1001–1007.
21. Levy C, et al. (2008) Molecular basis of halorespiration control by CprK, a CRP-FNR type transcriptional regulator. *Mol Microbiol* 70(1):151–167.
22. Bonnet M, et al. (2013) The structure of *Bradyrhizobium japonicum* transcription factor FixK2 unveils sites of DNA binding and oxidation. *J Biol Chem* 288(20):14238–14246.
23. Meister A, Anderson ME (1983) Glutathione. *Annu Rev Biochem* 52:711–760.
24. Masip L, Veeravalli K, Georgiou G (2006) The many faces of glutathione in bacteria. *Antioxid Redox Signal* 8(5-6):753–762.
25. Fahey RC (2013) Glutathione analogs in prokaryotes. *Biochim Biophys Acta* 1830(5):3182–3198.
26. Won HS, Lee YS, Lee SH, Lee BJ (2009) Structural overview on the allosteric activation of cyclic AMP receptor protein. *Biochim Biophys Acta* 1794(9):1299–1308.
27. Weber IT, Steitz TA (1987) Structure of a complex of catabolite gene activator protein and cyclic AMP refined at 2.5 A resolution. *J Mol Biol* 198(2):311–326.
28. Kabsch W (1993) Automatic processing of rotation diffraction data from crystals of initially unknown symmetry and cell constants. *J Appl Crystallogr* 26:795–800.
29. Bailey S; Collaborative Computational Project, Number 4 (1994) The CCP4 suite: Programs for protein crystallography. *Acta Crystallogr D Biol Crystallogr* 50(Pt 5):760–763.
30. Adams PD, et al. (2010) PHENIX: A comprehensive Python-based system for macromolecular structure solution. *Acta Crystallogr D Biol Crystallogr* 66(Pt 2):213–221.
31. Emsley P, Lohkamp B, Scott WG, Cowtan K (2010) Features and development of Coot. *Acta Crystallogr D Biol Crystallogr* 66(Pt 4):486–501.
32. McNicholas S, Potterton E, Wilson KS, Noble ME (2011) Presenting your structures: The CCP4mg molecular graphics software. *Acta Crystallogr D Biol Crystallogr* 67(Pt 4):386–394.
33. Berman HM, et al. (2000) The Protein Data Bank. *Nucleic Acids Res* 28(1):235–242.